Time-Accurate Simulations of a Shear Layer Forced at a Single Frequency

R. W. Claus*
NASA Lewis Research Center, Cleveland, Ohio
P. G. Huang†
Michigan Technological University, Houghton, Michigan
and
J. M. MacInnes‡
Princeton University, Princeton, New Jersey

This paper presents calculations of the forced shear layer studied experimentally by Oster and Wygnanski[1] and Weisbrot.[2] Two different computational approaches are examined: direct numerical simulation (DNS) and large eddy simulation (LES). The DNS approach solves the full three-dimensional Navier-Stokes equations for a temporally evolving mixing layer, while the LES approach (as applied in this work) solves the two-dimensional Navier-Stokes equations with a subgrid-scale turbulence model. While the comparison between these calculations and experimental data was hampered by a lack of information about the inflow boundary conditions, the calculations are shown to agree qualitatively with several aspects of the experiment. The sensitivity of these calculations to factors such as mesh refinement and Reynolds number is illustrated.

Introduction

GREAT interest has recently been directed toward the study of forced turbulent shear flows. Practically, the concern is with controlling the flow in order to achieve various desired results such as increased mixing. The hope is that through application of very low-amplitude (i.e., low-energy input) forcing one can significantly alter the flow development such that a large-amplitude effect is produced. Currently, our understanding of how these processes occur and how they can be manipulated is increasing dramatically, but significant questions remain. To take full advantage of the potential for controlling turbulence by forcing, a better understanding of the basic physics of the flowfield is needed. Specifically, the interaction of vortices of various scales must be more completely understood.

An excellent example of flowfield in which a wide range of vortices interact is the experiment studied by Oster and Wygnanski[1] and later by Weisbrot.[2] In this experiment a well-organized, periodic, large-scale motion is produced by forcing at a single frequency. The forced flow structure evolves in a turbulent flow, extracting energy from, and later returning energy to, the mean flow. The manner in which these large-scale structures interact with small-scale random motions (turbulence) yields a great deal of information on flow dynamics and presents an important challenge to those interested in predicting forced flows.

In this paper various numerical approaches are used to simulate the experiment of Ref. 2. One approach solves two-dimensional time-dependent equations for the phase-aligned motions and uses a two-equation turbulence model to represent the properties of the remaining (three-dimensional or nonaligned) motions. This approach, termed large eddy simulation (LES) in this report, assumes that the large-scale fluctuations in a shear layer are mainly two-dimensional and that the three-dimensional random motions can be represented by a turbulence model. Two-dimensional laminar flow calculations are also presented to provide a reference case for the LES calculations. The final computational approach examined is direct numerical simulation (DNS). With this approach the three-dimensional Navier-Stokes equations are solved for a temporally evolving shear layer. Each of these various computational approaches has unique advantages and disadvantages. The purpose of this report is to examine whether, in ensemble, these computations can predict the major features of the excited shear layer.

Computational Approach

Large Eddy Simulations

Several different computational approaches to making time-accurate calculations are employed in this report. The first approach, referred to here as a large eddy simulation (LES), solves the two-dimensional Navier-Stokes equations with a two-equation turbulence model. The turbulence model is used to represent the nonperiodic motion, while the large-scale motions are captured on a computational mesh. This methodology follows the Deardorff approach, which recognizes that the solution of the discretized equations using a finite-volume algorithm is mathematically equivalent to solving the original equations with a "box"-type filter.[3] The advantage of this approach is that the subgrid-scale turbulence model is significantly simplified. The (Leonard) stresses that arise through the use of a more general filter (e.g., a Gaussian filter) are zero. This permits the use of a turbulence model that is simply a time-dependent form of the commonly used Reynolds-averaged k-ϵ model.[4] There are some disadvantages to this approach, and Ref. 5 is recommended as a source detailing these issues. It is sufficient to state that at this time it is not clear that any significant penalties are incurred through the use of this approach.

Presented as Paper 88-0061 at the AIAA 26th Aerospace Sciences Meeting, Reno, NV, Jan. 11–14, 1988; received May 7, 1988; revision received Feb. 24, 1989.

*Aerospace Engineer, Internal Fluid Mechanics Division. Member AIAA.
†Assistant Professor, Mechanical Engineering and Engineering Mechanics.
‡Research Staff Member, Mechanical and Aerospace Engineering.

The numerical scheme used to solve the discretized equations is an implicit incompressible flow algorithm. Flow variables are represented on a staggered mesh with Crank-Nicholson time differencing and QUICK differencing[6] of the convective terms. This approach maintains second-order accuracy in both time and space. Continuity is enforced through the iterative pressure-correction scheme SIMPLE (Semi-Implicit Pressure Linked Equations).[7] The computer code is described in detail by its originators in Ref. 8. It has undergone extensive testing and evaluation in idealized benchmark problems[9] and numerous practical flow calculations. For the present work modifications were made to the code to improve vectorization, and a more efficient solver, employing Stone's strongly implicit algorithm combined with a block correction, is used to solve the pressure-correction equation.[10]

In applying this code to the time-dependent shear-layer calculations, the domain extends from the transverse plane, which is just at the trailing edge of the splitter plate (Fig. 1), and extends the full length of the experimental test section. Boundary conditions for u, v, k, and ϵ at the inlet are prescribed according to estimates of the experimental conditions. The upper and lower boundaries were treated as imposed symmetry conditions. At the domain exit, a zero-gradient outflow boundary condition is applied to each variable. As shown in Ref. 11, the use of this type of outflow boundary condition should contaminate the flowfield near the outflow but should not significantly affect the locations where the computational results are compared to experimental data.

The strongest gradients in these calculations occur in the central region of the flow domain and have a dominant y-direction component. To accommodate these gradients one-third of the mesh points in the y direction are uniformly distributed in the central 10% of the domain. The remaining two-thirds are divided among the upper and lower portions with variable spacing so that a smooth transition is made at the interfaces. In the finest mesh used, the streamwise x direction is resolved with 798 grid points and the y direction with 241 points, which will be described in the abbreviated manner 798 × 241 grid points. The grid point spacing was expanded 0.1% per grid cell in the axial direction. The expansion factor for the coarsest-mesh calculations (150 × 80 grid points) was 0.267%, and the expansion factor for the 400 × 241-mesh calculations was 0.2%. These mesh points were distributed over a range of 0–2000 mm in the x direction and −200–+200 mm in the y direction.

The shear layer is known as a convectively unstable type of flow.[12] This means that the small perturbations upstream grow exponentially as they are convected with the flow. For this reason it was recognized that the treatment of the inflow boundary condition was very important in establishing a correct comparison with experimental data. Unfortunately, detailed measurements near the splitter plate were not available, so it was necessary to estimate the thickness of the boundary layers as they left the splitter plate. A momentum thickness (θ) estimate of 0.5 mm for the layer on each side of the splitter plate was inserted into an exponential profile:

$$u = u_\infty \exp\{-(y - y_0)/2\theta\}, \qquad y_0(t) = Y \sin \omega t$$

$$v = 0$$

where the oscillation of the plate position is y_0 at the experimental frequency, $\omega = 45$ Hz, and amplitude Y simulates the effect of the flapping metal strip placed at the trailing edge of the splitter plate in the experiment. The freestream velocities are 10 m/s and 6 m/s in the two separate supply streams. Numerically, a number of different inflow boundary profiles were simulated. Without examining an infinite number of permutations, the profile described here was selected as reasonably representative of experimental conditions. But it is certainly true that the calculations are very sensitive to this boundary condition, and it is appropriate here to emphasize the importance of documenting the details of the inlet flow for an experiment to provide useful information for testing calculations.

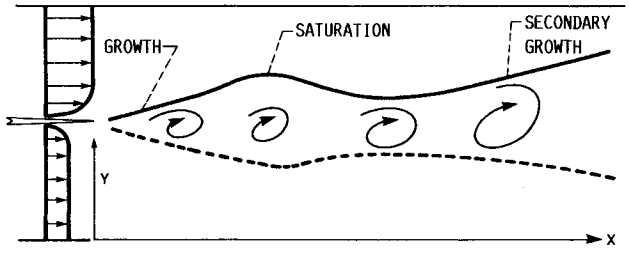

Fig. 1. Two-dimensional flow geometry showing the orientation of the axes and major flowfield features.

Inlet conditions for the turbulence model were somewhat easier to establish. The experiment documented a streamwise turbulence intensity of around 0.2%, so $k \simeq \overline{u'^2} = 4 \times 10^{-4}$ m^2/s^2 is used. The length scale of the turbulence entering the test section was not documented but can be estimated from the formula $\epsilon = k^{3/2}/l$ using a length scale on the order of $l \simeq 2$ mm. Fortunately, some test calculations indicate that the results are not sensitive to the precise value of ϵ used, within a reasonable range.

As noted previously, these are incompressible flow calculations wherein a perturbation anywhere in the flowfield can be "felt" everywhere else in the flow. Practically, what this requires is that the calculations be run for a long time period to allow the initial conditions of the flow to be completely "flushed" through the computational domain until periodic flow behavior is reached. This is partially affected by the level of mass residual allowed in the iterative calculation, where the lower the residual, the faster the approach to periodicity. The laminar flow calculations were much more sensitive to this effect and generally had to be run for longer flow times to reach periodicity.

Laminar Flow Calculations

These calculations are identical to those described previously, except that a constant molecular viscosity is used in place of the turbulence model viscosity. The Reynolds number based on the mean convective velocity and the wavelength of forcing was 96,000.

Direct Numerical Simulations

The term direct numerical simulation as used here refers to the solution of the three-dimensional, time-dependent Navier-Stokes equations by a highly accurate numerical scheme such that all the scales of motion are well-resolved on a computational mesh. This imposes two major restrictions on this computational scheme. First, although highly accurate spectral methods are used to solve the governing equations, only a limited range of fluctuating motions can be resolved on the computational mesh. This restricts the calculations to a low Reynolds-number flow (approximately 50–100 based on the Taylor microscale). When one applies the results of a low Reynolds-number calculation to understand high Reynolds-number turbulence, an inherent assumption is that the large energetic scales of turbulent motion display characteristics that are independent of Reynolds number. The second major limitation of these direct numerical simulations is that the use of spectral methods (Fourier series) imposes the need to use periodic boundary conditions in the main flow direction. This means that these calculations correspond to a temporally evolving shear layer as opposed to the spatial evolution of the experiment. A Galilean transformation[13] can be applied that relates the statistics of the time-evolving shear layer to spatial experimental data. This translation uses the average convective velocity to relate the statistics at one time (in the temporal simulation) to an axial distance downstream. This transformation is a good approximation of the laboratory

experiment when the average convective velocity is much greater than the velocity difference between the two streams. For the experiment in Ref. 2, this condition is only approximated. As a consequence, these time-evolving simulations should be looked at as approximations or "idealizations" of the real flow. The drawback that this time-evolving description of the flow imposes in comparisons with experimental data is offset by the increased numerical resolution available in the calculation.

Results and Discussion

The flow geometry and the main features of the forced flowfield are illustrated in Fig. 1. Initially, the shear layer is subject to very rapid growth due to the rollup of vortices scaling with the forcing wavelength. Somewhat further downstream the rollup process saturates and the shear layer stops growing. This is followed by a collapse of the layer width and then by a slow, secondary growth. These are the principle characteristics of the flowfield documented in Ref. 2 that will be compared with the results of numerical simulations.

The results of two-dimensional laminar flow calculations are displayed in Fig. 2. In general, the calculations display the development of both positive and negative vorticity as the boundary layers leave the splitter plate and form large-scale structures. The positive vorticity regions (dashed contours) result from the low-speed boundary layer used as an inflow boundary condition. This positive vorticity is rapidly dissipated as the mean flow gradient encourages the formation of negative vorticity.

The effect of grid resolution can be seen in the instantaneous vorticity contours in Figs. 2a and 2b. The coarse-mesh calculation initially forms two small discrete vortices (around 400 mm) that rapidly coalesce into one larger vortex of a scale corresponding to the wavelength of the periodic forcing. The fine-mesh calculation initially forms many more smaller-scale vortices, and approximately six of these vortices slowly coalesce and merge into a single-vortex structure very near the exit of the computational domain. The fine-mesh calculation retains much higher levels of negative vorticity throughout the flowfield, indicating improved numerical resolution.

These marked differences between the fine- and coarse-mesh calculations indicate that the calculations are not mesh-independent. For at least the laminar flow calculations it appears that mesh refinement yields very small-scale detail in the near field that can significantly affect the development of the flow. Even the high level of mesh refinement present in the calculation with 798×241 mesh points is probably insufficient to fully resolve this flowfield. The inflow boundary conditions impose a very sharp gradient in the velocity profile, providing a ready source of ever smaller-scale vorticity. The actual experimental values may not be this severe, but lacking experimental data, a definitive evaluation cannot be made.

The Reynolds stress field averaged over one cycle of the imposed forcing is displayed in Fig. 2c. The dashed lines indicate regions of negative Reynolds stress where the energy transfer is from the fluctuating motions to the mean flow: the so-called "inverse cascading" seen in forced flows. Small regions of negative stress appear first on the low-speed side of the layer and then later on the high-speed side. These small regions of negative stress are caused by individual small vortices changing their orientation with respect to the main flow. Downstream from these isolated pockets of negative stress, a large region of negative stress is formed due to the orientation of the whole vortex ensemble. This is the region where the layer undergoes a "collapse" and noticeably reduces in thickness. Downstream from the large region of negative

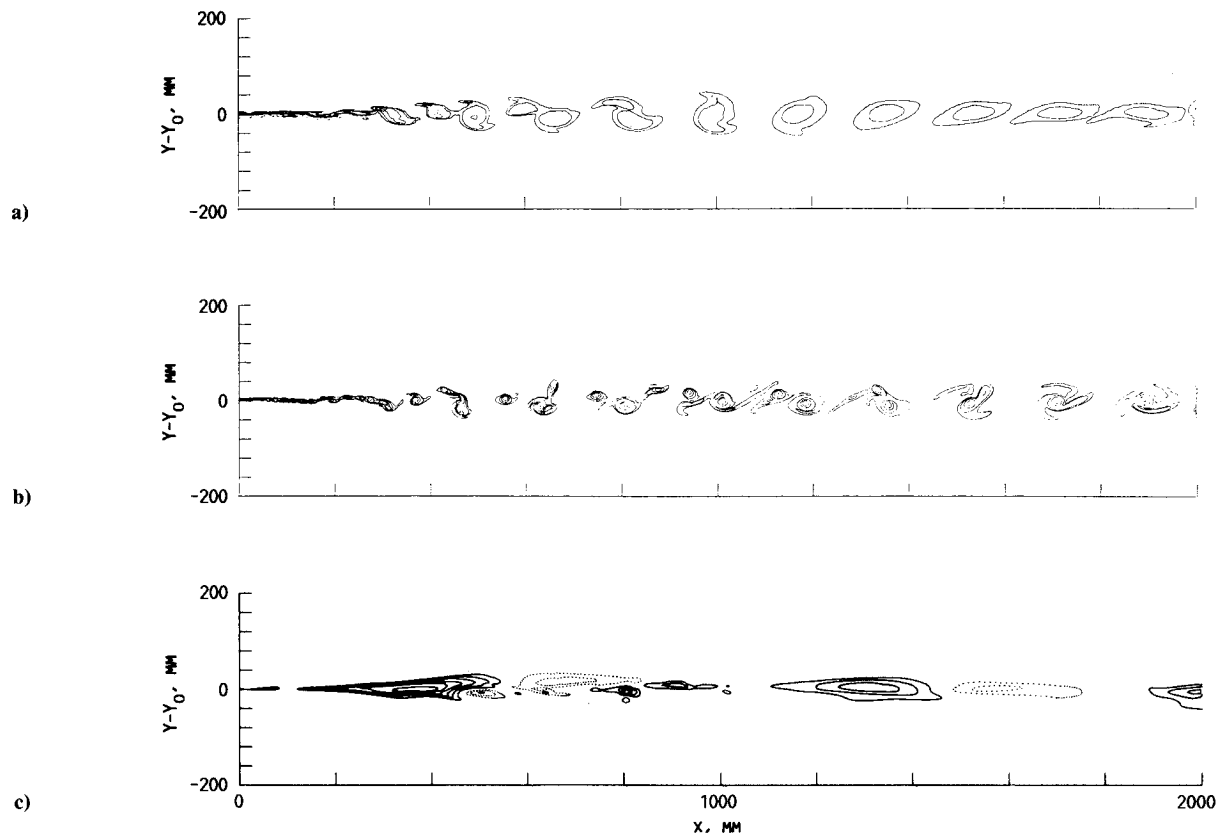

Fig. 2 Computational results for the two-dimensional laminar flow calculations: a) instantaneous vorticity for a coarse-mesh calculation (150×80 grid points), contours of -500, -250, -100, -50, and dashed $+50$, $+100$; b) instantaneous vorticity for a fine-mesh calculation (798×241 grid points), contours of -500, -250, -100, -50, and dashed $+50$, $+100$; c) averaged Reynolds stresses ($-\overline{uv}/\Delta U^2$) of the oscillatory motion (798×241 grid points). Contours range from solid lines, 0.015 to 0.090 in intervals of 0.015, and dashed lines, -0.045 to -0.015 in intervals of 0.015.

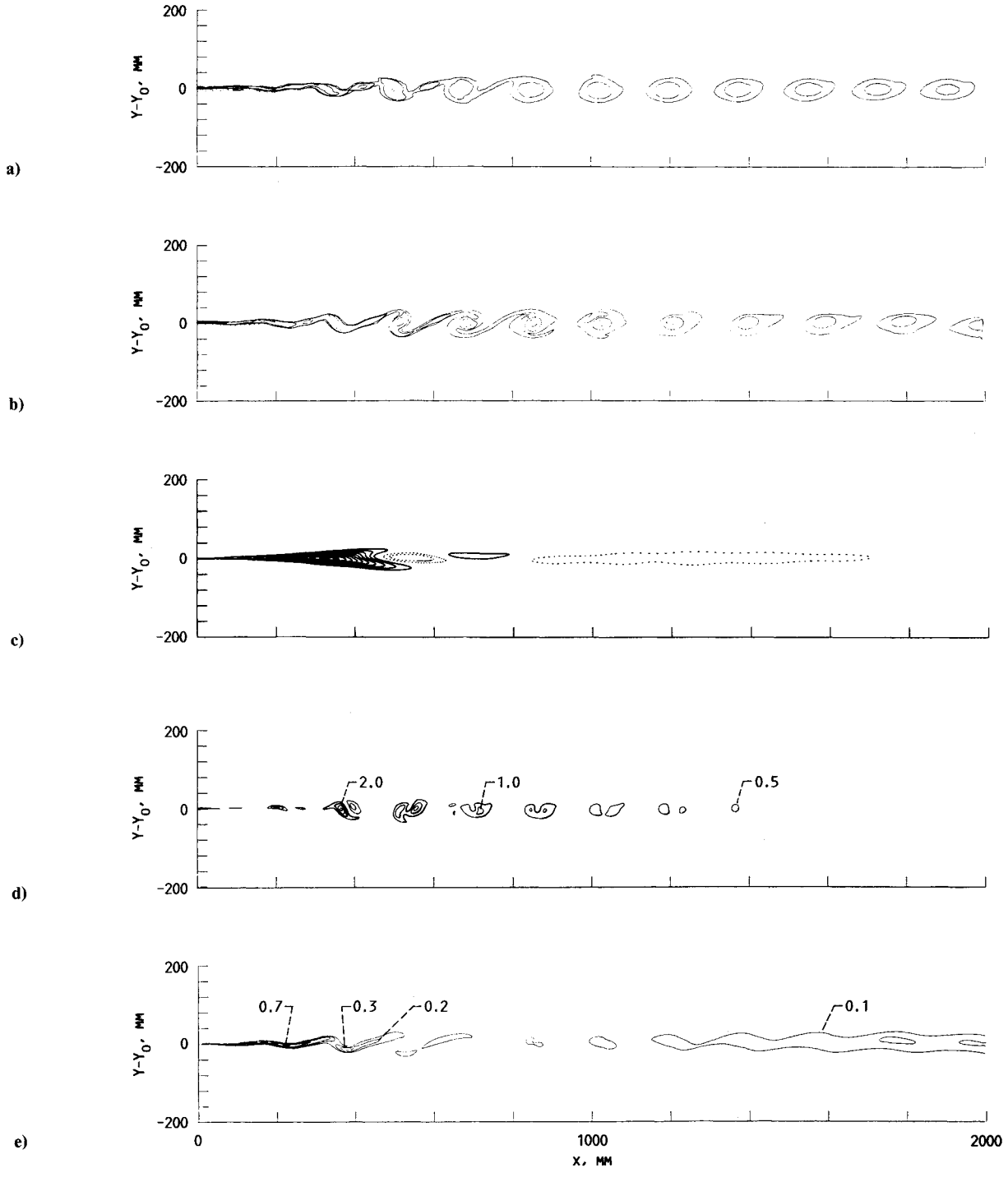

Fig. 3 Computational results of the LES calculations (400 × 241 grid points unless noted): a) instantaneous vorticity for a coarse-mesh calculation (150 × 80 grid points), contours of −500, −250, −100, −50, and dashed +50, +100; b) instantaneous vorticity for a fine-mesh calculation (400 × 241 grid points), contours of −500, −250, −100, −50, and dashed +50, +100; c) averaged Reynolds stresses ($-\overline{uv}/\Delta U^2$) of the oscillatory motion (400 × 241 grid points). Contours range from solid lines, 0.0075 to 0.0750; and d) instantaneous kinetic energy of the oscillatory motion (k = 0.5 to 3.0 in increments of 0.5); e) instantaneous turbulence kinetic energy from the turbulence model (k = 0.1 to 0.7 in increments of 0.1).

stress, the flow alternates between positive and negative stress as the large-scale forced structure exhibits vortex nutation.

The LES calculations, shown in Fig. 3, are significantly different from the laminar flow calculations. In general, the contours of vorticity display a much more organized (or smooth) flow pattern than the fine-mesh laminar flow calculations. The effective viscosity added by the turbulence model serves to damp out most of the small-scale features that form near the inflow boundary. The only remaining structure is the periodic structure associated with the forcing. This structure rapidly forms and then dissipates as it travels downstream.

Figures 3a and 3b display the results of LES calculations for two different mesh densities. These results indicate less sensitivity to mesh refinement compared to the laminar calculation, but there is still some grid dependency. It is interesting that the fine-mesh calculation appears smoother than the coarse-mesh calculation near the inflow boundary. Apparently, the reduction in numerical diffusion in the fine-mesh

calculation is more than offset by the increased turbulence generation produced by the model in response to sharper velocity gradients.

The averaged Reynolds stresses (evaluated from the oscillatory component of motion only) are shown in Fig. 3c. These stresses are much more uniform than those in the laminar flow calculations. A large region of positive stress near the inflow boundary changes to low levels of negative stress further downstream. About halfway through the flowfield the stresses become negative and remain negative, though gradually being dissipated as the exit is approached. In this final region of the flow the effect of the turbulence model has been to diffuse vorticity and thereby slow down the interaction between the vorticity and the mean flow. This decreases the rate at which the stresses change sign.

Of course, the oscillatory motion in the LES calculations represents only a part of the total turbulent kinetic energy in the calculation—the turbulence model supplies the rest. The magnitude of these two different components of the kinetic energy can be compared using the instantaneous contours displayed in Figs. 3d and 3e. In general, the kinetic energy in the oscillatory motion is much greater than that supplied by the turbulence model, especially in the middle of the flow domain. Near the inflow boundary, where mean gradients are quite steep, the turbulence model displays its highest levels of kinetic energy. Near the outflow boundary the kinetic energy associated with the turbulence model is of the same approximate level as that of the oscillatory motion. One interesting feature of the turbulence model kinetic energy is that local maxima are observed in regions of the flow commonly referred to as the braids. These are regions of intense shear that have been experimentally shown to be the source of counter-rotating, streamwise vortices that are a major component of three-dimensional "random" turbulence in shear layers.[14] It is certainly encouraging that, while the LES calculation is purely two-dimensional, the turbulence model (that is intended to represent all other fluctuations) does concentrate random motion energy in the braid region, similar to experimental findings. To establish whether this effect is quantitatively correct would require more detailed experimental measurements.

A "close-up" comparison between these calculations and the experimental data is shown in Figs. 4–6. Figure 4 compares the instantaneous vorticity contours in the region from $x = 200$ to 560 mm. (Contour levels were not documented in the reported experimental data. The computational contour levels were chosen to reveal the main features of the flow and should not be expected to display the same density of lines as in the experiment.) In this region of the flow, near the splitter plate, the initial stage of the vortex rollup may be seen. Experimentally, the initial vortex displays a number of vorticity maxima (perhaps three or four), and the next vortex (around 440 mm) displays two maxima. The laminar flow calculation displays many more vorticity maxima, and the structure of the second vortex, especially, is markedly different. The LES calculation dissipates the small-scale vortices so that only a few maxima are seen (approximately one per structure). The LES calculation appears to show too little small-scale structure, while the laminar flow calculation shows too much.

Figure 5 displays the instantaneous vorticity contours in the region between axial locations of 560 and 840 mm. Again, as in the previous figure, the laminar flow calculation displays too much small-scale structure. The LES calculation displays two very smooth vortices, which is roughly in agreement with the experimental contours.

Figure 6 displays the instantaneous vorticity contours between axial locations of 840 and 1780 mm. Again, the laminar flow calculation displays too much small-scale structure and, near the end of the region (around 1700 mm), a double-vortex structure is seen. In the LES calculations the effect of dissipation can be seen through the decreasing density of the vorticity contours. A similar trend is seen in the experimental data with the exception that the large structure appears now to be composed of two nearly vertically aligned vortices.

From these various close-up comparisons it appears that the LES calculation is initially too dissipative near the inflow boundary or close to the splitter plate. Further on, in the

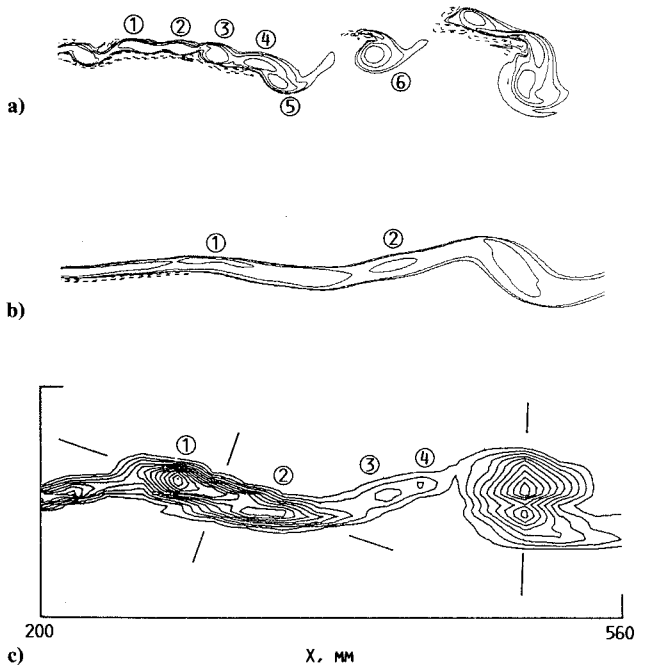

Fig. 4. Instantaneous vorticity contours for the two-dimensional calculations and experimental data around axial locations of 200 to 560 mm: a) laminar calculation (798 × 241 grid points); b) LES calculation (400 × 241 grid points); c) experiment, Ref. 2.

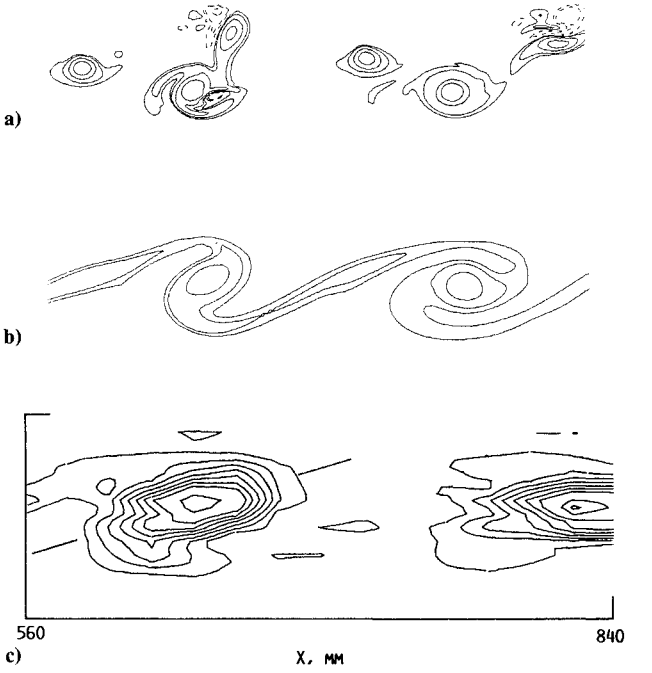

Fig. 5. Instantaneous vorticity contours for the two-dimensional calculations and experimental data around axial locations of 560 to 840 mm: a) laminar calculation (798 × 241 grid points); b) LES calculation (400 × 241 grid points); c) experiment, Ref. 2.

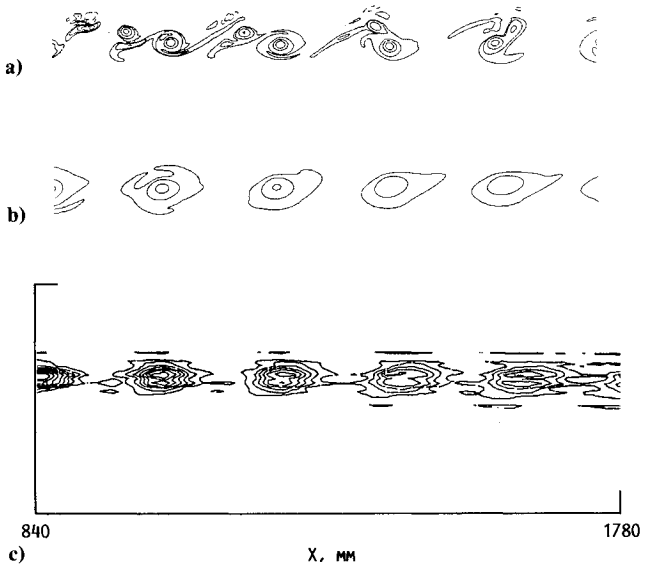

Fig. 6. Instantaneous vorticity contours for the two-dimensional calculations and experimental data around axial locations of 840 to 1780 mm: a) laminar calculation (798 × 241 grid points); b) LES calculation (400 × 241 grid points); c) experiment, Ref. 2.

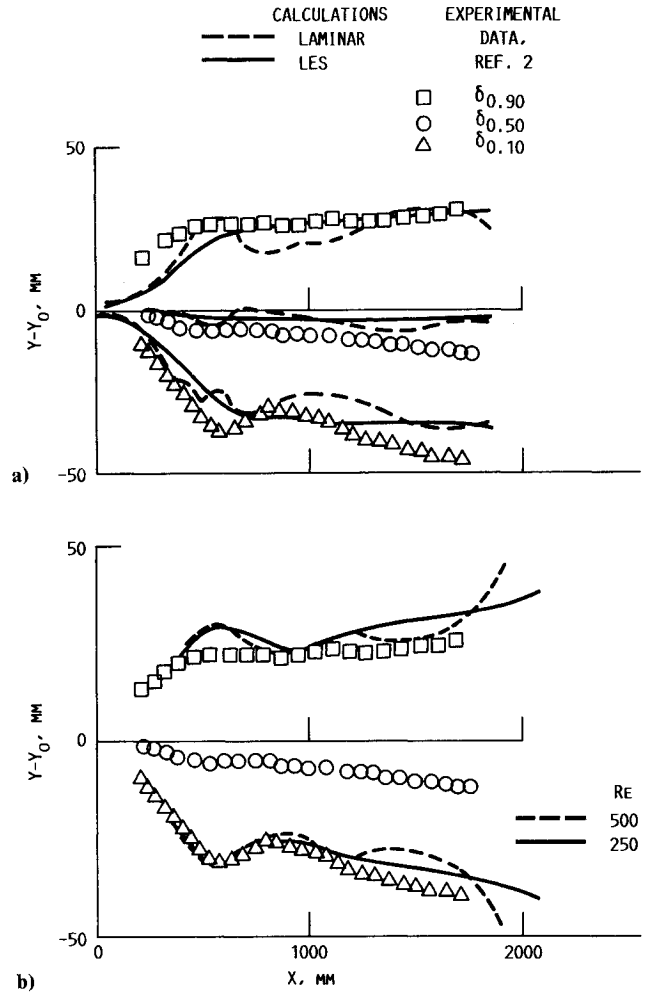

Fig. 7. Comparison of calculated and experimentally measured mean axial velocity development. $\delta_{0.x}$ = radial location where the flow reaches x% of $U_{-\infty}$ or $U_{+\infty}$: a) laminar and LES calculations; b) DNS calculations for two different initial Reynolds numbers (64 × 64 × 64 grid points).

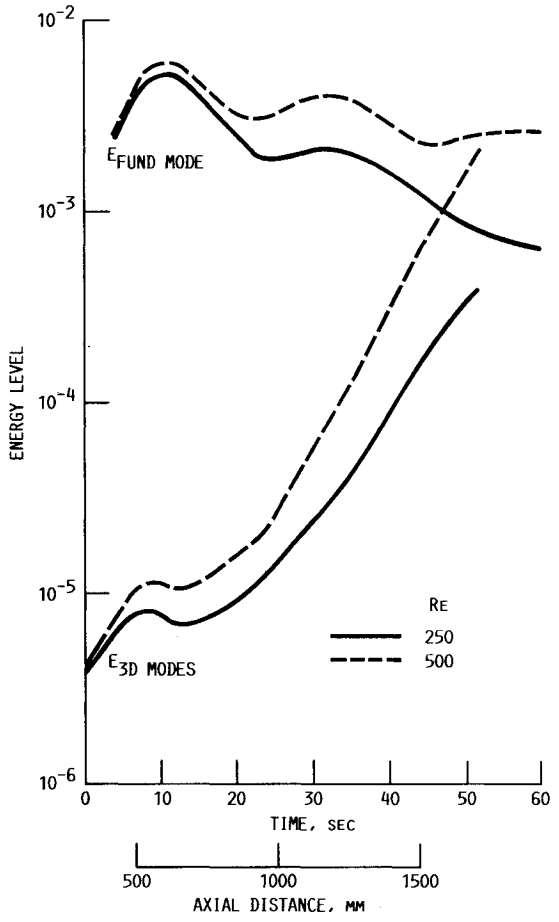

Fig. 8. Energy content of various modes in the DNS calculations for two different Reynolds numbers (64 × 64 × 64 grid points).

free-shear region of the flow, the turbulence model appears to provide approximately the correct level of diffusion. This suggests that some mechanism may be needed to modify the dissipation rate equation such that the behavior in the near wake of the boundary layer is less dissipative.

A comparison of calculated and experimentally measured mean axial velocity layer position as a function of downstream distance is shown in Fig. 7. Figure 7a presents the two-dimensional LES and the laminar flow calculations. In general, both computations grow too rapidly in the initial portion of the flowfield but appear to saturate at approximately the same point as the experimental data. The laminar calculations reveal saturation of several small vortices leading to the "bumpy" nature of the velocity-layer growth. The LES calculation exhibits a very smooth velocity-layer growth, but the sharp collapse of the layer, seen experimentally, is not reproduced in the calculation. Neither of the calculations appears to indicate the slow secondary growth on the low-velocity side.

Figure 7b compares DNS calculations made at two different initial Reynolds numbers with the experimental data. The low Reynolds-number ($Re = 250$) results compare quite favorably with the low-speed side of the velocity profile. Unfortunately, the DNS results are symmetric about the centerline and cannot capture the difference between the high- and low-speed sides of the layer. The layer growth at the higher Reynolds number ($Re = 500$) is very similar to that at the lower Reynolds number, except for the region near the end of the computations, where the layer growth suddenly becomes quite rapid. This is in contrast to the slow secondary growth found in the experiment. As will be shown in the next figure, this region of very strong growth coincides with the emer-

gence of three-dimensional streamwise vortices that lead to a cascade of energy toward smaller scales. The energy built up at these smaller scales cannot be resolved on the computational mesh, and for longer time periods (beyond those noted in Fig. 7b), the DNS calculation becomes meaningless. This is a characteristic weakness of the DNS approach (as noted earlier), but the trends indicated by the calculation should be valid.

The energy content of various modes in the DNS calculations is shown in Fig. 8 for the two different Reynolds numbers. The fundamental mode (the excited wave) and the three-dimensional modes (streamwise vortices) are the primary structures in this flowfield. The fundamental mode grows rapidly early in the calculation and is largely unaffected by Reynolds number. Around a time of 10 s (or 600 mm) the fundamental mode saturates and then, primarily, loses energy. In this region of decay of the fundamental mode, the three-dimensional modes gain energy very rapidly. This trend is strongly affected by Reynolds number. Essentially what is occurring is that the two-dimensional spanwise structure (the fundamental mode) is strongly stretching the three-dimensional counter-rotating vortices that form in the braid region of the flow. This feature of the flow is graphically documented in Ref. 15. The growth of the streamwise structures causes a growth in the mean thickness of the shear layer.

A comparison of calculated and experimentally measured Reynolds stresses is shown in Fig. 9. The various computational approaches display very different trends. In general, none of the calculations is quantitatively correct, although the DNS and LES calculations always display the correct sign. The LES stress is a combination of that associated with the oscillatory motion and that contributed by the turbulence model. The turbulence model does not significantly contribute to the Reynolds stresses at $x = 440$ or 720 mm, but it is significant enough at $x = 1700$ mm to change the sign of the stresses from negative to positive. The LES calculations match the experimental data very closely at $x = 440$ mm but are in poorer agreement with the measurements downstream. The laminar calculations approximate the data at $x = 440$ mm but are also in poorer agreement further downstream. The worst agreement is exhibited at $x = 1700$ mm by the laminar calculations, where the sign of the stresses is incorrect.

The experimental data also include information on the Reynolds stresses contributed by the oscillatory forced structure. This information was obtained by taking measurements that were "phase-locked" at the frequency of forcing. The stresses contributed by the forced structure could then be separated from the total stresses obtained by long-time averaging. Figure 10 displays the phase-locked (or oscillatory) and total stresses measured experimentally at $x = 1700$ mm. These results are compared with the LES and DNS calculations. In the case of the DNS calculations, the total stresses are presented for two different Reynolds numbers. The main difference in these two results is the strength of the three-dimensional modes (or the streamwise vortices) as seen in Fig. 8. At the higher Reynolds number the streamwise vortices are strong enough to cause the stresses to be significantly positive. At the lower Reynolds number the stresses are so small as to

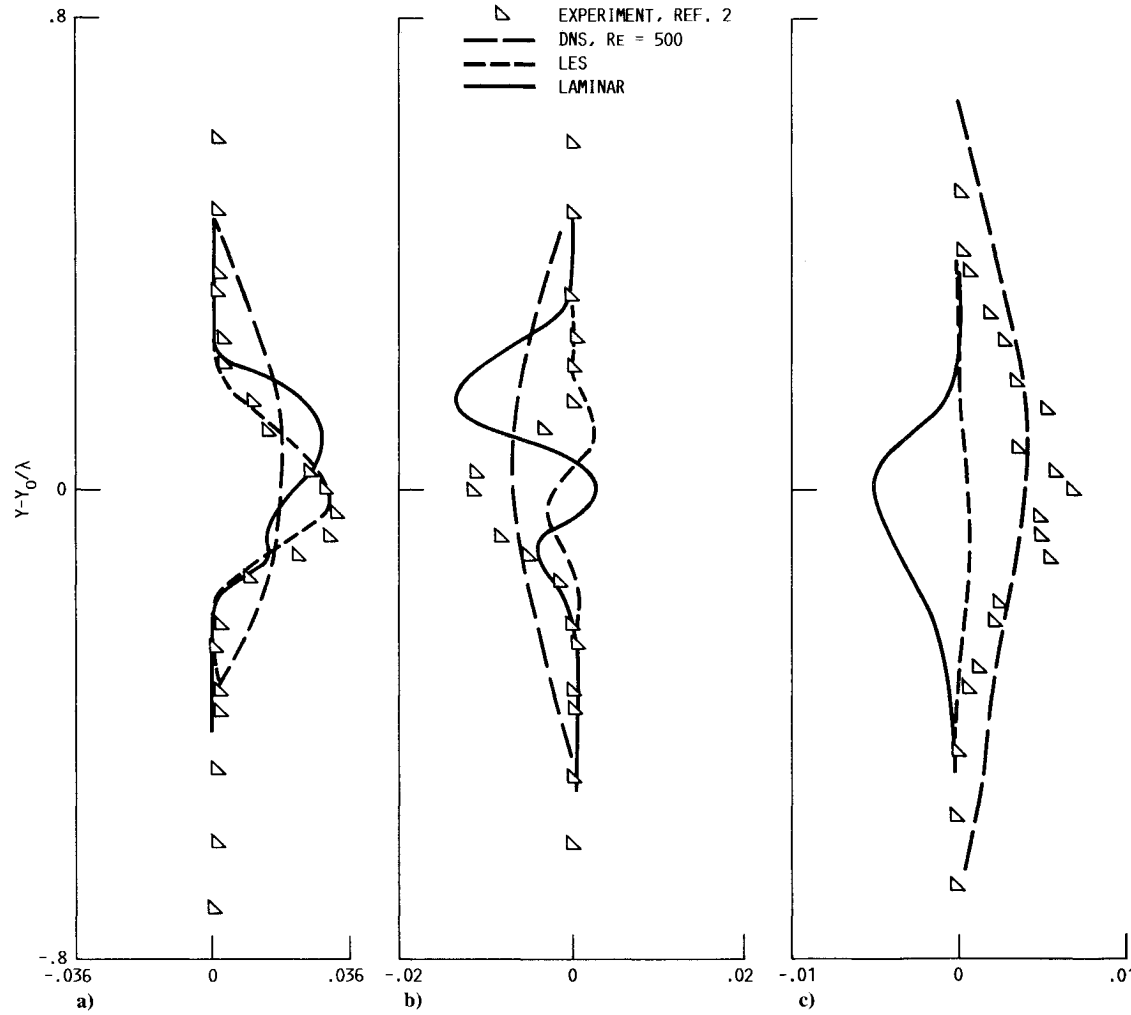

Fig. 9 Comparison of calculated and experimentally measured total Reynolds stresses at several axial locations. λ = wavelength of forcing: a) $x = 440$ mm; b) $x = 720$ mm; c) $x = 1700$ mm.

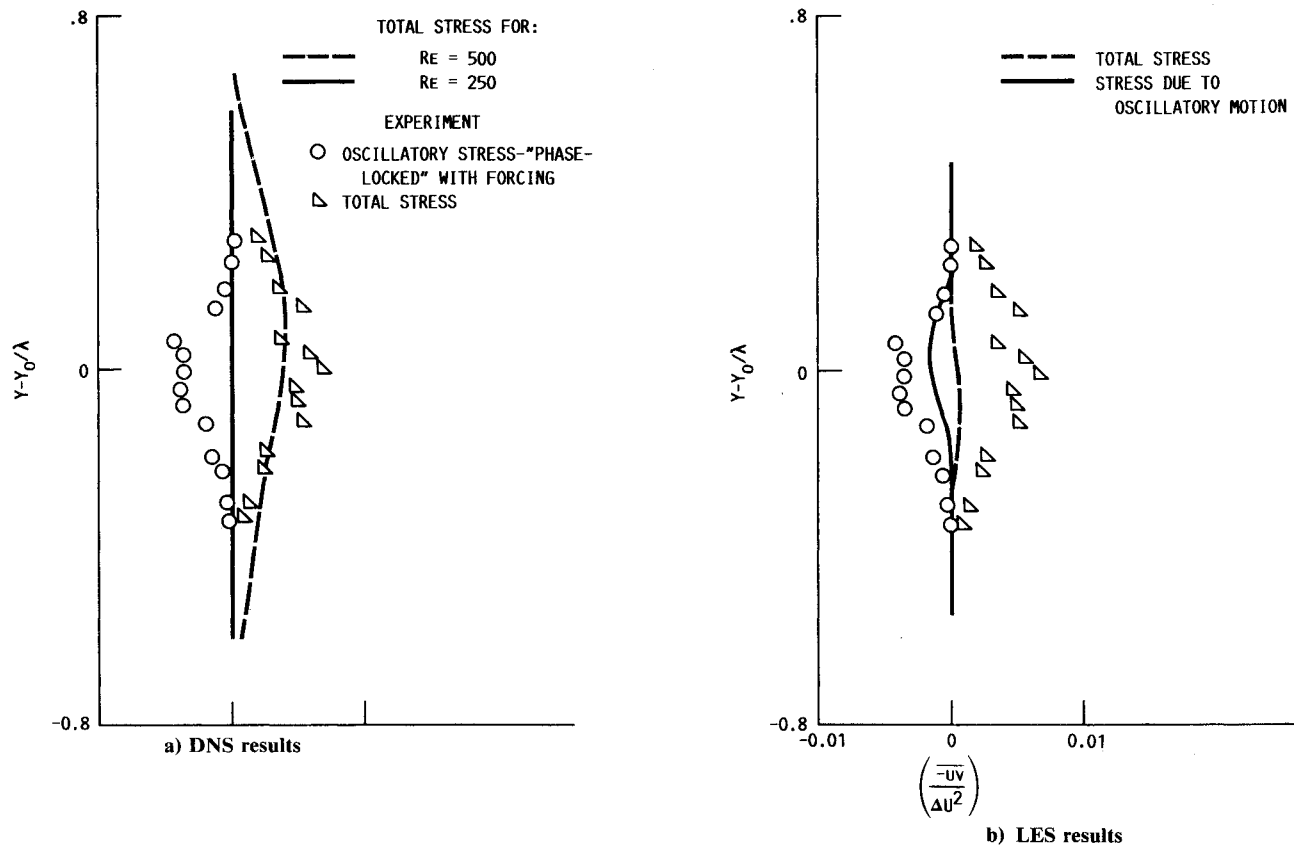

Fig. 10 Total and oscillatory Reynolds stresses (experimentally measured at $x = 1700$ mm) compared with LES and DNS calculations. The oscillatory stresses are phase-locked to the forcing wavelength. λ = wavelength of forcing.

be effectively zero across the layer. The LES calculations indicate that the stresses due to the oscillatory motion are negative, while the total stresses (a combination of the oscillatory motion and turbulence model stresses) are positive. While the LES results are in qualitative agreement with the experiment, the magnitude of the calculated stresses is much smaller than in the experiment.

Concluding Remarks

At this point it is appropriate to restate the question implicitly posed in the introduction to this paper. In ensemble, can the various computational approaches examined predict the major features of the excited shear layer? Lacking detailed measurements of the inflow boundary conditions, it is impossible to definitively answer this question. Certainly the initial growth and saturation of the shear layer are approximated by all of the methods. The laminar and the LES calculations display very different small-scale behavior, but the initial rollup is largely dominated by the forced structure and all the calculations represent this feature. From this point in the flow, however, the DNS calculations indicate that small-scale, streamwise vortices grow very rapidly. This transition from two-dimensional forced motion to three-dimensional and, eventually, rather random motion seems likely to be the cause of the slow secondary growth found experimentally. The LES calculations do display increased levels of turbulence kinetic energy in the braid regions where the streamwise structures originate, but this has no significant effect on the mean flow. The oscillatory motion dominates the stresses in the LES calculations up until very near the outflow. Near the outflow, the turbulence model significantly alters the stresses to the extent that the negative stresses contributed by the oscillatory motions are entirely offset, making the total stresses positive. Although this trend is in agreement with the experimental data, it is quantitatively too small to significantly affect the mean velocity profile and display some secondary growth. The DNS calculations may overestimate the importance of the streamwise vortices due to their inability to cascade energy to scales both larger than the computational domain and smaller than the computational mesh.

The final point to be emphasized is the importance of mesh refinement. Although new supercomputers have made possible the fine-mesh calculations reported here, it is likely that these results (at least for laminar flow) remain grid-dependent. This grid dependency can strongly alter the calculated vorticity structure and the development of the flow.

Acknowledgments

The authors are listed alphabetically. The use of the NAS Cray 2 for all of these calculations is gratefully acknowledged.

References

[1]Oster, D. and Wygnanski, I., "The Forced Mixing Layer Between Parallel Streams," *Journal of Fluid Mechanics*, Vol. 123, Oct. 1982, pp. 91–130.

[2]Weisbrot, I., "A Highly Excited Turbulent Mixing Layer," M.S. Thesis, Tel Aviv University, Dept. of Fluid Mechanics and Heat Transfer, 1984; see also Weisbrot, I. and Wygnanski, I., "On Coherent Structures in a Highly Excited Mixing Layer," *Journal of Fluid Mechanics*, Vol. 195, Oct. 1988, pp. 137–160.

[3]Deardorff, J. W., "A Numerical Study of Three-Dimensional Turbulent Channel Flow at Large Reynolds Number," *Journal of Fluid Mechanics*, Vol. 41, 1970, pp. 452–480.

[4]Launder, B. E. and Spalding, D. B., "The Numerical Computation of Turbulent Flows," *Computer Methods in Applied Mechanics and Engineering*, Vol. 3, 1974, pp. 269–289.

[5]Ferziger, J. H., "Higher Level Simulations of Turbulent Flows," *Computational Methods for Turbulent, Transonic, and Viscous Flows*, Hemisphere, New York, 1983, pp. 93–182.

[6]Leonard, B. P., "Stable and Accurate Convective Modelling Procedure Based on Quadratic Upstream Interpolation," *Computer*

Methods in Applied Mechanics and Engineering, Vol. 19, June 1979, pp. 59–98.

[7]Patankar, S. V. and Spalding, D. B., "A Calculation Procedure for Heat, Mass and Momentum Transfer in Three-Dimensional Parabolic Flows," *International Journal of Heat and Mass Transfer*, Vol. 15, No. 10, Oct. 1972, pp. 1787–1806.

[8]Huang, P. G. and Leschziner, M. A., "An Introduction and Guide to the Computer Code TEAM," Thermofluids Division Technical Rept. TFD/83/9(r), University of Manchester Institute of Science and Technology, Department of Mechanical Engineering, 1983.

[9]Huang, P. G., Launder, B. E., and Leschziner, M. A., "Discretization of Nonlinear Convection Processes: A Broad Range Comparison of Four Schemes," *Computer Methods in Applied Mechanics and Engineering*, Vol. 48, Feb. 1985, pp. 1–24.

[10]Turan, A. and VanDoormal, J. P., "Improved Numerical Methods for Turbulent Viscous Recirculating Flows," NASA CR-180852, 1987.

[11]Korczak, K. Z. and Hu, D., "Turbulent Mixing Layers—Direct Spectral Element Simulation," AIAA Paper 87-0133, 1987.

[12]Bechert, D. W., "Excitation of Instability Waves," *Zeitschrift fuer Flugwissensehaften und Weltraumforschung*, Vol. 9, 1985, pp. 356–361.

[13]Orszag, S. A. and Pao, Y. H., "Numerical Computation of Turbulent Shear Flows," *Advances in Geophysics*, Vol. 18A, 1974, pp. 225–236.

[14]Hussain, A. K. M. F. and Zaman, K. B. M. Q., "An Experimental Study of Organized Motions in the Turbulent Plane Mixing Layer," *Journal of Fluid Mechanics*, Vol. 159, 1985, pp. 85–104.

[15]Claus, R. W., "Direct Numerical Simulations of a Temporally Evolving Mixing Layer Subject to Forcing," NASA TM-88896, 1986.